

## Research Article

# A Study on Seismic Isolation of Shield Tunnel Using Quasi-Static Finite Element Method

Can Li <sup>1,2,3</sup>, Weizhong Chen <sup>1</sup>, Wusheng Zhao <sup>1</sup>, Takeyasu Suzuki <sup>4,5</sup>  
and Yoshihiro Shishikura<sup>3</sup>

<sup>1</sup>State Key Laboratory of Geomechanics and Geotechnical Engineering, Institute of Rock and Soil Mechanics, Chinese Academy of Sciences, Wuhan, Hubei 430071, China

<sup>2</sup>University of Chinese Academy of Sciences, Beijing 100049, China

<sup>3</sup>Graduate School of Engineering, Civil and Environment Engineering Course, University of Yamanashi, 4-3-11 Takeda, Kofu, Yamanashi 400-8511, Japan

<sup>4</sup>Graduate School of Interdisciplinary Research, University of Yamanashi, 4-3-11 Takeda, Kofu, Yamanashi 400-8511, Japan

<sup>5</sup>Disaster and Sustainable Administration Research Center, University of Yamanashi, 4-3-11 Takeda, Kofu, Yamanashi 400-8511, Japan

Correspondence should be addressed to Weizhong Chen; wzchen@whrsm.ac.cn and Wusheng Zhao; zhusheng@163.com

Received 10 December 2018; Revised 7 January 2019; Accepted 20 February 2019; Published 2 May 2019

Academic Editor: Hamid Toopchi-Nezhad

Copyright © 2019 Can Li et al. This is an open access article distributed under the Creative Commons Attribution License, which permits unrestricted use, distribution, and reproduction in any medium, provided the original work is properly cited.

Using a quasi-static method based on an axisymmetric finite element model for seismic response analysis of seismically isolated tunnels, the seismic isolation effect of the isolation layer is studied, and the seismic isolation mechanism of the isolation layer is clarified. The results show that, along the longitudinal direction of the tunnel, the seismic isolation effect is mainly affected by the shear modulus of the isolation material. The smaller the shear modulus is, the more evident the seismic isolation effect is. This is due to the tunnel being isolated from deformation of its peripheral ground through shear deformation of the isolation layer. However, along the transverse direction of the tunnel, the seismic isolation effect is mainly affected by the shear modulus and Poisson's ratio of the isolation material. When Poisson's ratio is close to 0.5, a seismic isolation effect is not evident because the tunnel cannot be isolated from deformation of its peripheral ground through compression deformation of the isolation layer. Finally, a seismic isolation system comprising a shield tunnel in which flexible segments are arranged at both ends of an isolation layer is proposed, and it is proved that the seismic isolation system has significant seismic isolation effects both on the longitudinal direction and on the transverse direction.

## 1. Introduction

Shield tunnels are widely used for water supply, public transport, communication, sewerage, and other infrastructures. Tunnels do not cause self-excited vibration under earthquakes but rather are controlled by the surrounding ground deformation. Therefore, it is generally recognized that tunnels are not easily affected by earthquakes. In recent years, with the increase in the number of underground structures and the frequent occurrence of seismic damage to underground structures, the antiseismic issue of underground structures is increasingly attracting high attention from seismologists around the world.

As shown in Figure 1, the seismic isolation layer applied to a tunnel is a technology to reduce the seismic response of the tunnel by isolating the tunnel body from deformation of the ground in the outer periphery of the structure. The effectiveness of the seismic isolation layer has been verified by a series of numerical simulations and experiments [1–4]. Seismic response analysis of tunnels is divided into cross-sectional seismic response analysis of tunnels and seismic response analysis of tunnels as a whole. At present, there are many methods for seismic response analysis of tunnels; typical ones include the Bessel function approximate solution, the response displacement method, and the finite element dynamic analysis method. The Bessel function

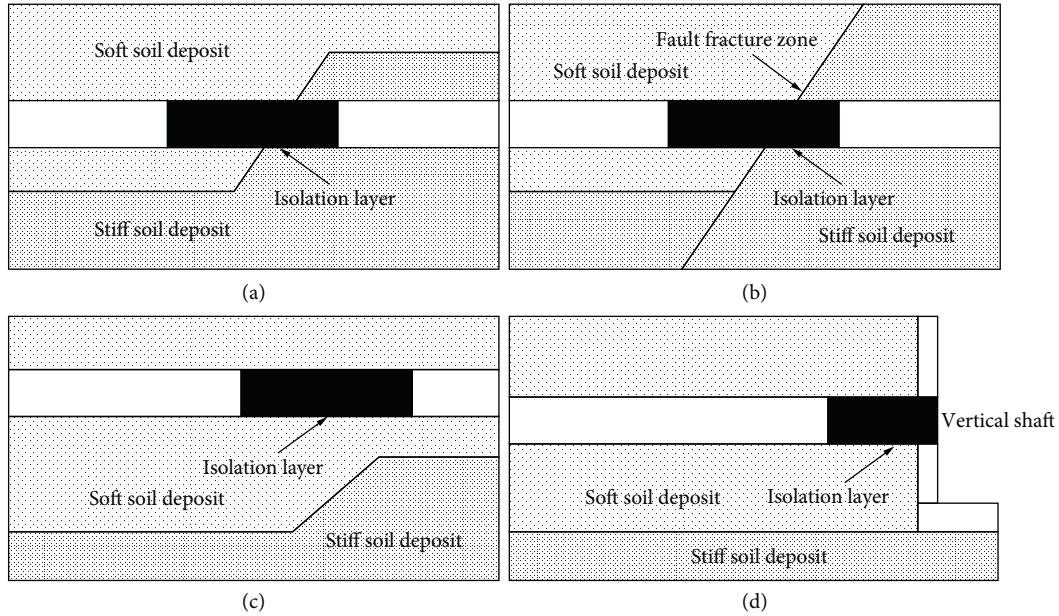


FIGURE 1: Concepts of a seismic isolation layer for shield tunnels. (a) Traversing the boundary between a soft soil deposit and a stiff soil deposit; (b) traversing a fault fracture zone; (c) underlying boundary between a soft soil deposit and a stiff soil deposit; (d) junction with a vertical shaft.

approximate solution is mainly suitable for cross-sectional seismic response analysis of tunnels, without dynamic analysis of the surrounding ground, and establishment of a new structural model of the tunnel. The approximate solution of the tunnel lining internal force of a circular cross section can be obtained using a theoretical formula. The analytic target and external force are based on ideal assumption. In the case of a sudden change in ground conditions, the approximate analytical Bessel function solution for general ground cannot give the internal force of the tunnel lining correctly. Under this condition, it is necessary to use other analytic methods [5, 6]. The response displacement method is suitable for cross-sectional seismic response analysis of tunnels and seismic responses of tunnels as a whole at the same time. The tunnel lining is simulated as a ring beam for the cross-sectional seismic analysis or the straight beam for the whole longitudinal seismic analysis. The ground spring, showing the interaction between the tunnel lining and surrounding ground, is placed around the tunnel lining, and the surrounding ground response displacement and shear stress are input into one end of the ground spring. This method is practical. However, due to the complexity of ground conditions, it is difficult to set up the ground spring, and the beam-spring model used for seismic design of underground pipelines does not necessarily give a good approximation for tunnels with large diameters, so it has limitations [7, 8]. In the finite element dynamic nonlinear analytic method, it is needed to consider various nonlinear questions, and the modeling process is complicated. It requires very large calculation resources and time, especially in three-dimensional analysis. Meanwhile, it is difficult to provide strict dynamic boundary conditions. Hence, it is not suitable for practical seismic isolation design of tunnels [9, 10].

The behavior of a tunnel subjects to deformations imposed by the surrounding ground. At present, the research on seismic isolation of tunnels mainly focuses on tunnel cross sections. However, as a linear underground structure, the key point is to study the seismic isolation of tunnel as a whole. The whole longitudinal behavior of a tunnel subjected to deformations imposed by the surrounding ground can be divided into two types [11]: (1) compressive and tensile deformations along the longitudinal direction (Figure 2(a)) and (2) bending deformation along the transverse direction (Figure 2(b)). In this paper, a quasi-static method based on an axisymmetric finite element model for seismic response analysis of seismically isolated tunnels is used to research the seismic isolation effect and mechanism of seismic isolation layer of a shield tunnel along both the longitudinal and transverse directions.

## 2. Quasi-Static Method for Seismic Response Analysis of Seismically Isolated Tunnels

**2.1. Outline of the Quasi-Static Method.** The quasi-static approach adopting an axisymmetric FEM and the response acceleration method is used for practical design of seismically isolated tunnels; this approach eliminates the troublesome processing of boundary conditions related to reflected waves and modeling complex ground and structural conditions.

It is well known that the response acceleration method provides slightly better evaluations than the finite element dynamic analysis approach; that is, the method presents more reliable and safer evaluation results. This method has been adapted to the seismic design of underground ducts, shafts, and rock caverns. In this method, the

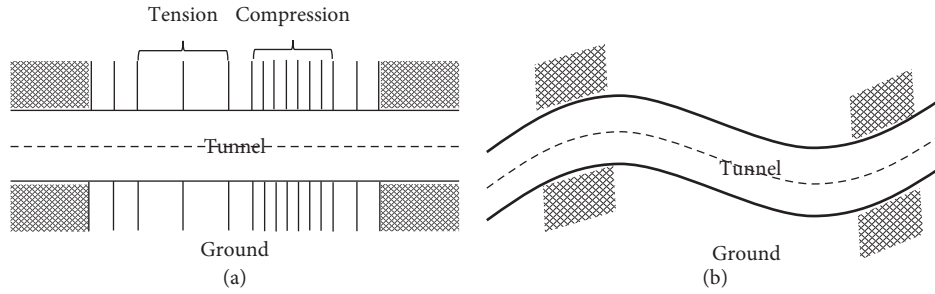


FIGURE 2: Deformation modes of tunnels due to seismic waves. (a) Longitudinal direction and (b) transverse direction.

surrounding ground is modeled by means of finite elements, and accelerations are calculated in a free field. The calculated accelerations are then applied to the finite element model, including an underground structure [12–14].

Figure 3 illustrates a schematic representation of the axisymmetric modeling. In the upper part of the figure, a tunnel is constructed through a soil deposit, while the lower part represents the axisymmetric modeling of the ground and tunnel conditions shown in the upper part; here, the centerline of the tunnel is set as an axis of symmetry. It is essential that special considerations should be taken when modeling the effects of the ground surface, boundary conditions, and seismic load. Accordingly, if a method can be defined to convert the seismic load in the axisymmetric model, thereby equalizing the ground displacements around the tunnel shown in the upper and lower parts of Figure 3, a simplified procedure can be developed to evaluate the 3-D interaction effects around a tunnel.

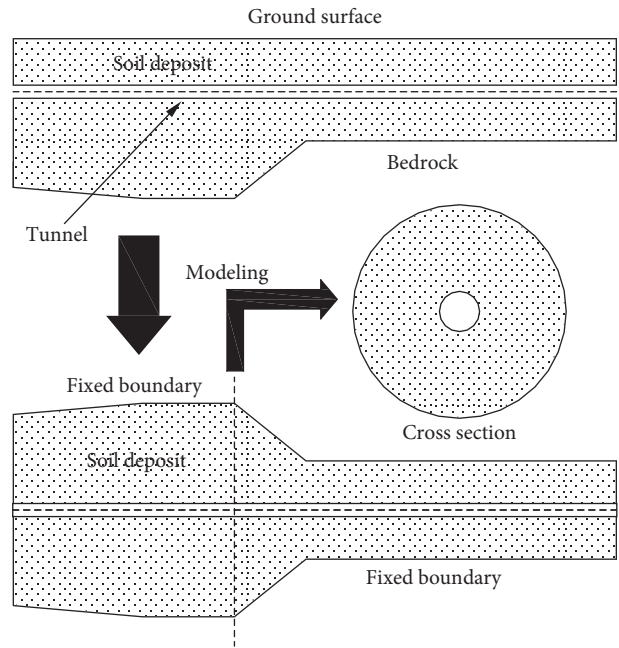


FIGURE 3: Schematic illustration of axisymmetric modeling.

**2.2. Method to Convert the Seismic Load.** The fundamental theory regarding the method employed to determine the seismic load in the axisymmetric model will be described in this section. The corresponding underground and loading conditions are shown in Figure 4, where  $H$  denotes the thickness of the soil deposits,  $z$  denotes the coordinate originating from the bedrock, and  $h_c$  denotes the height from the bedrock to the tunnel center under actual tunnel and ground conditions. In the axisymmetric model, an axis of symmetry is located at the height of the upper outer surface of the actual tunnel, and the outer radius  $R$  denotes the distance from the axis to the bedrock. The outer surface of the axisymmetric model corresponding to the outer surface of the tunnel lining is located at the radius  $r = r_0$ , where  $r_0$  denotes the outer radius of the tunnel lining. Then,  $h_c$  and  $R$  can be related by  $h_c = R - r_0$ . The seismic load considered here is an inertial force originating from the ground acceleration due to seismic ground motions. The static loading method, in which the inertial force due to an earthquake is loaded statically while ignoring the damping term in the equations of motion, is employed herein.

Figure 5 illustrates a schematic diagram to describe the method of applying an inertial seismic load on the ground.

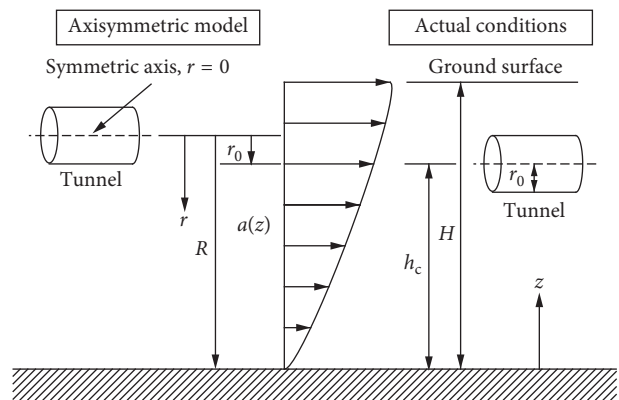


FIGURE 4: Coordinates of the axisymmetric model in comparison with the coordinates under actual conditions.

In the proposed model, the seismic load is divided into two components: an inertial force denoted  $P(z)$ , which is given in equation (1), acting on the ground beneath the tunnel and a concentrated force  $S$ , which is given in equation (2), acting on the outer surface of the tunnel body:

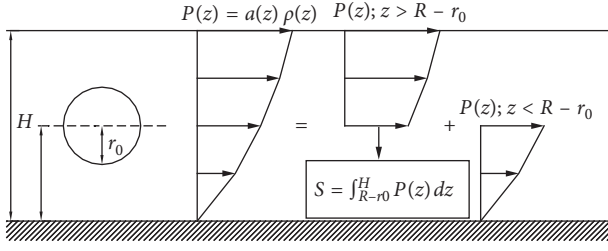


FIGURE 5: Method employed to apply a seismic load.

$$P(z) = a(z)\rho(z), \quad (1)$$

$$S = \int_{R-r_0}^H P(z) dz. \quad (2)$$

The conversion of the seismic load in the axisymmetric model is conducted as shown in Figure 5.

**2.2.1. Seismic Load in the Longitudinal Direction.** The conversion of the seismic load in the longitudinal direction is conducted in the following manner [15, 16]. The displacement of the ground at  $z$  with the unit width is defined as  $u$  when the horizontal force  $P$  is acting at a height  $z$ . The displacement at  $r (=R - z)$  of a hollow cylindrical disk with a unit thickness, the outer surface of which is constrained, is defined as  $u^*$  when the horizontal force  $P^*$  is acting at  $r$ . Placing the displacements  $u^*$  and  $u$  equal to each other,  $P^*$  can be expressed using  $P$ ,  $R$ , and  $r$  as follows:

$$P^* = \frac{2\pi(R-r)}{\ln(R/r)} P(z; R-r). \quad (3)$$

The concentrated force  $S$  in equation (2) can also be replaced by  $S^*$  as shown below:

$$S^* = \frac{2\pi(R-r_0)}{\ln(R/r_0)} S. \quad (4)$$

Figures 6(a) and 6(b) represent the relation between the concentrated force and ground shear deformation in the actual ground and in the axisymmetric model, respectively; the case of a soil column is shown in Figure 6(a), and the case of a hollow cylindrical disk is shown in Figure 6(b). The shear displacement values at the location  $r=r_0$  in Figure 6(a) and the shear displacement values at the location  $z=h_c$  in Figure 6(b) are coincident with each other. However, the shape of the vertical shear displacement distribution in the hollow cylindrical disk in Figure 6(b) is not straight and is widely different from that in the soil column displayed in Figure 6(a). To make the vertical distribution of the shear displacement in the proposed model equal to that in the actual ground, the following method is adopted.

When the concentrated load  $S^*$  acts on  $r=r_0$ , the shear displacement  $u_c$  is

$$u_c = \frac{S^*}{2\pi G} \ln \frac{R}{r_0}. \quad (5)$$

However, as shown in Figure 7, assuming that the acceleration is uniformly distributed in the vertical direction, the inertial force  $s_i^*$  is

$$s_i^* = a \cdot \pi \rho_i (r_i^2 - r_{i-1}^2). \quad (6)$$

When the inertial force  $s_i^*$  acts on a hollow cylindrical disk with a unit thickness ranging from  $r_{i-1}$  to  $r_i$ , the shear displacement  $u_{c,i}$  produced by the inertial force is

$$u_{c,i} = \frac{s_i^*}{2\pi G} \ln \frac{R}{r_i}. \quad (7)$$

Then, the shear displacement produced at  $r=r_0$  is

$$u_c = \sum_{i=2}^n u_{c,i}. \quad (8)$$

The uniformly distributed acceleration, which can be derived from equation (8), is given by equation the following equation:

$$a = \frac{2\pi(R-r_0)}{\pi \cdot \sum_{i=2}^n [\rho_i (r_i^2 - r_{i-1}^2) \cdot \ln(R/r_i)]} S. \quad (9)$$

In numerical analysis, earthquake loads acting at  $r$  are calculated by multiplying the mass matrix by the ground acceleration at  $r$ . Thus, the acceleration at  $r$  used in such calculations can be given by equation (10), which is derived from equations (3) and (9); this acceleration denoted  $a(r)$  used herein is defined as a modified acceleration coefficient:

$$a(r) = a + \frac{2\pi(R-r)}{\ln(R/r)} a(z; R-r). \quad (10)$$

Finally, by applying the inertial force, which is the product of the mass  $m(r)$  and acceleration  $a(r)$  of each node as the seismic load, the displacement generated in the actual ground can be reproduced. In the analysis of the longitudinal direction, the load acts in the longitudinal direction on each hollow cylindrical disk as an axisymmetric load.

**2.2.2. Seismic Load in the Transverse Direction.** The conversion of the seismic load in the transverse direction is conducted in the following manner. The displacement of the ground at  $z$  with the unit width is defined as  $u$  when the horizontal force  $P$  is acting at a height  $z$ . The displacement at  $r (=R - z)$  of a hollow cylindrical disk with a unit thickness, the outer surface of which is constrained, is defined as  $u^*$  when the horizontal force  $P^*$  is acting at  $r$ . Placing the displacements  $u^*$  and  $u$  equal to each other,  $P^*$  can be expressed using  $P$ ,  $R$ , and  $r$  as follows:

$$P^* = \frac{8\pi \cdot (3-4\nu)(1-\nu)(R-\nu)}{(3-4\nu)^2 \ln(R/r_0) - \left[ \frac{(R/r_0)^2 - 1}{(R/r)^2 + 1} \right]} \cdot P(z; R-r). \quad (11)$$

The concentrated force  $S$  in equation (2) can also be replaced by  $S^*$  as follows:

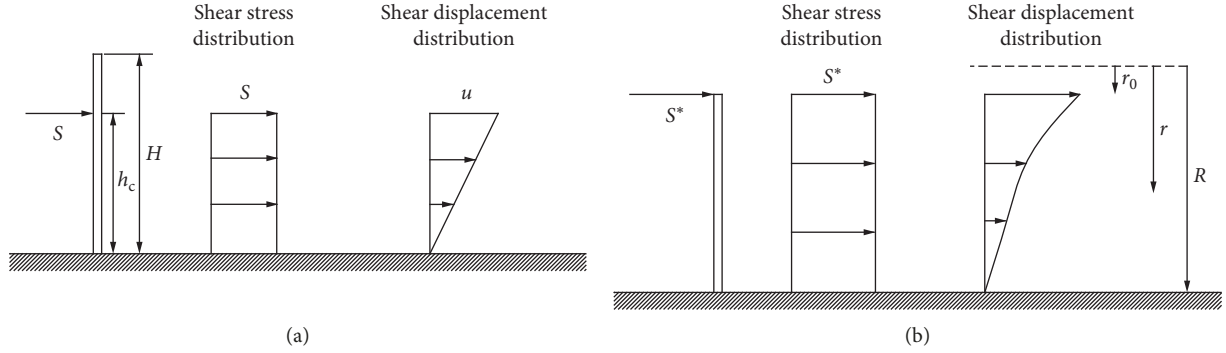


FIGURE 6: Relationship between the concentrated force and ground shear deformation along the longitudinal direction of a tunnel in (a) the actual ground and (b) the axisymmetric model.

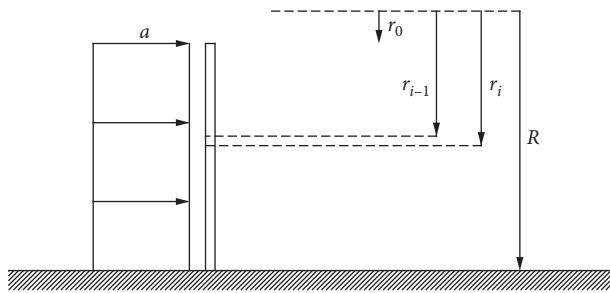


FIGURE 7: Conversion of the concentrated load  $S^*$  along the longitudinal direction of a tunnel.

$$S^* = \frac{8\pi \cdot (3-4\nu)(1-\nu)(R-r_0)}{(3-4\nu)^2 \ln(R/r_0) - \left( \left[ \frac{(R/r_0)^2 - 1}{(R/r_0)^2 + 1} \right] \right)} S. \quad (12)$$

Figures 8(a) and 8(b) represent the relation between the concentrated force and ground shear deformation in the actual ground and the axisymmetric model, respectively; the case of a soil column is shown in Figure 8(a), and the case of a hollow cylindrical disk is shown in Figure 8(b). The shear displacement values at the location  $r = r_0$  in Figure 8(b) and the shear displacement values at the location  $z = h_c$  in Figure 8(a) are coincident with each other. However, the vertical shear displacement distribution in the hollow cylindrical disk displayed in Figure 8(b) is not straight and is widely different from that in the soil column illustrated in Figure 8(a). To make the vertical distribution of the shear

displacement in the proposed model equal to that in the actual subsurface, the following method is adopted.

When the concentrated load  $S^*$  acts on  $r = r_0$ , the shear displacement  $u_c$  is

$$u_c = \frac{(3-4\nu)^2 \ln(R/r_0) - \left( \left[ \frac{(R/r_0)^2 - 1}{(R/r_0)^2 + 1} \right] \right)}{8\pi \cdot (3-4\nu)(1-\nu) \cdot G} S^*. \quad (13)$$

However, as shown in Figure 9, assuming that the acceleration is uniformly distributed in the vertical direction, the inertial force  $s_i^*$  is

$$s_i^* = a \cdot \pi \rho_i (r_i^2 - r_{i-1}^2). \quad (14)$$

When the inertial force  $s_i^*$  acts on a hollow cylindrical disk with a unit thickness ranging from  $r_{i-1}$  to  $r_i$ , the shear displacement  $u_{c,i}$  produced by the inertial force is

$$u_{c,i} = \frac{(3-4\nu)^2 \ln(R/r_i) - \left( \left[ \frac{(R/r_i)^2 - 1}{(R/r_i)^2 + 1} \right] \right)}{8\pi \cdot (3-4\nu)(1-\nu) \cdot G} s_i^*. \quad (15)$$

Then, the shear displacement produced at  $r = r_0$  is

$$u_c = \sum_{i=2}^n u_{c,i}. \quad (16)$$

The uniformly distributed acceleration  $a$ , which can be derived from equation (16), is given by the following equation:

$$a = \frac{8\pi \cdot (3-4\nu)(1-\nu)(R-r_0)}{\pi \cdot \sum_{i=2}^n [\rho_i (r_i^2 - r_{i-1}^2)] \cdot \sum_{i=2}^n \left\{ (3-4\nu)^2 \ln(R/r_i) - \left( \left[ \frac{(R/r_i)^2 - 1}{(R/r_i)^2 + 1} \right] \right) \right\}} S. \quad (17)$$

In numerical analysis, an earthquake load acting at  $r$  is calculated by multiplying the mass matrix by the ground acceleration at  $r$ . Thus, the acceleration at  $r$  used in such calculations can be given by equation (18), which is derived from equations (11) and (17); the acceleration  $a(r)$  used herein is defined as a modified acceleration coefficient:

$$a(r) = a + \frac{8\pi \cdot (3-4\nu)(1-\nu)(R-r)}{(3-4\nu)^2 \ln(R/r) - \left( \left[ \frac{(R/r)^2 - 1}{(R/r)^2 + 1} \right] \right)} \cdot a(z; R-r). \quad (18)$$

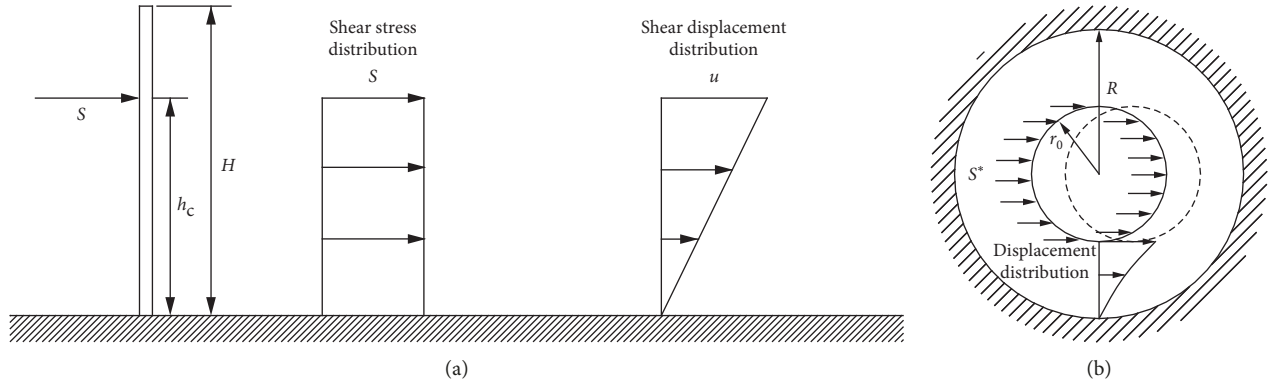


FIGURE 8: Relationship between the concentrated force and ground shear deformation along the transverse direction of a tunnel in (a) the actual ground and (b) the axisymmetric model.

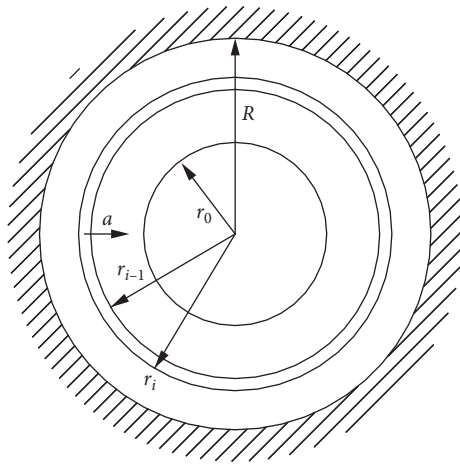


FIGURE 9: Conversion of the concentrated load  $S^*$  along the transverse direction of a tunnel.

Finally, by applying the inertial force, which is the product of the mass  $m(r)$  and acceleration  $a(r)$  at each node as the seismic load, the displacement generated in the actual ground can be reproduced in the axisymmetric model. In the analysis of the transverse direction, the load acts in the transverse direction on each hollow cylindrical disk as an asymmetrical load.

### 3. Seismic Isolation Effect and Mechanism of the Isolation Layer

**3.1. Modeling of Shield Tunnels and Method for Determining Calculation Parameters.** A shield tunnel is a structure formed by segments, which are fastened by joints. For reasonably showing the shield tunnel characteristics, joint effects should be included when modeling a shield tunnel. An equivalent stiffness beam model of the shield tunnel is often used in the actual shield tunnel design. As shown in Figure 10, based on the equivalent stiffness beam model, the calculation parameters of the shield tunnel finite element in the axisymmetric finite element model are determined.

The equivalent stiffness of the shield tunnel can be calculated using the following equation:

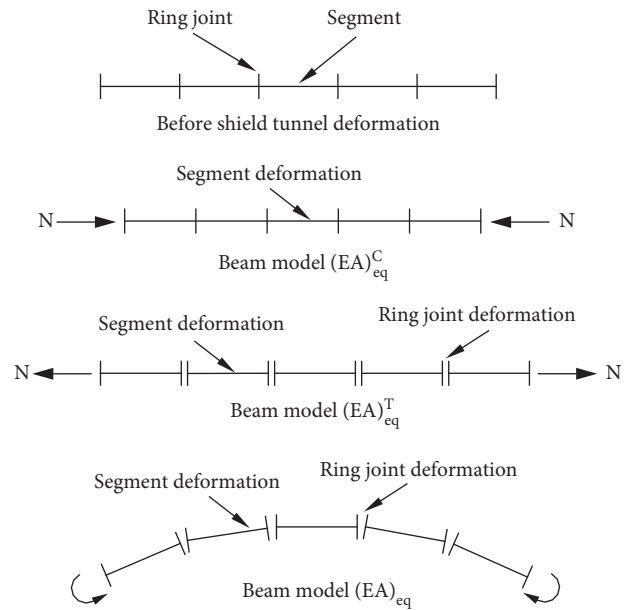


FIGURE 10: Schematic diagram of the equivalent stiffness beam model for a shield tunnel.

$$(EA)_{eq}^C = E_s \cdot A_s,$$

$$(EA)_{eq}^T = \frac{1}{(E_s \cdot A_s / l_s \cdot K_j) + 1} \cdot E_s \cdot A_s,$$

$$(EI)_{eq} = \frac{\cos^3 \varphi}{\cos \varphi + ((\pi/2) + \varphi) \cdot \sin \varphi} \cdot E_s \cdot I_s, \quad (19)$$

$$\varphi + \cot \varphi = \pi \cdot \left( \frac{1}{2} + \frac{K_j}{E_s \cdot (A_s / l_s)} \right),$$

where  $(EA)_{eq}^C$  is the equivalent compression stiffness,  $(EA)_{eq}^T$  is the equivalent tension stiffness,  $(EI)_{eq}$  is the equivalent bending stiffness,  $l_s$  is the segment width,  $A_s$  is the cross-sectional area of the segment,  $E_s$  is the elastic modulus of the segment,  $K_j$  is the sum of the tension stiffness of the spring of ring joints,  $I_s$  is the moment of inertia of the segment

section, and  $\varphi$  is the angle corresponding to where the neutral axis of segment section exists.

Therefore, the elastic modulus of the finite elements of shield tunnel lining in the axisymmetric finite element model is as follows:

$$\begin{aligned} E_C &= \frac{(EA)_{eq}^C}{A_s}, \\ E_T &= \frac{(EA)_{eq}^T}{A_s}, \\ E_I &= \frac{(EI)_{eq}}{I_s}, \end{aligned} \quad (20)$$

where  $E_C$  is the compression elastic modulus,  $E_T$  is the tension elastic modulus, and  $E_I$  is the bending elastic modulus.

**3.2. Research on the Seismic Isolation Effect of Isolation Layers.** As shown in Figure 11, to study the seismic isolation effect of the isolation layer, seismic response analyses are conducted on cases in which an isolation layer is applied to a shield tunnel buried in irregularly bounded surface soil deposits, and the results of these analyses are compared in this paper. A shield tunnel with an outer diameter of 5.1 m made of reinforced concrete segments with a thickness of 25 cm constructed in the place where ground conditions change sharply is considered. Because the outer diameter of the shield machine was 5.2 m, the thickness of the isolation layer was set to 10 cm, which equals the thickness of the tail void. Table 1 reports the equivalent stiffness of the shield tunnel. Figure 12 shows the discretization and boundary conditions of the axisymmetric finite element mesh. In the axisymmetric model, the mesh is discretized into 9 layers in the circumferential direction. The lining and isolation layer are each modeled by a layer.

As shown in Figure 13, the input earthquake motion for Level 2 earthquake motion was chosen from among standard waves used for seismic design of road bridges [17]. Waves obtained by performing amplitude of the EW component at JR Takatori Station were used as Type II earthquake motion for category II ground, which is a motion originated from a near-fault earthquake.

Seismic isolation materials suitable for underground structures should have certain physicochemical properties, and the most important thing to consider is whether the existence of an isolation layer will affect the static stability of underground structures. A softer isolation layer has a more evident seismic isolation effect; however, considering the uneven settlement of ground, Poisson's ratio of the isolation material should be close to 0.5. When Poisson's ratio of the isolation material is close to 0.5, uneven settlement of the ground can be avoided effectively, even if the isolation material is very soft [18]. In this paper, silicone material (SISMO), recommended for seismic isolation design of shield tunnels, is used as the isolation material for numerical simulations. Its shear elastic modulus is relatively small, and

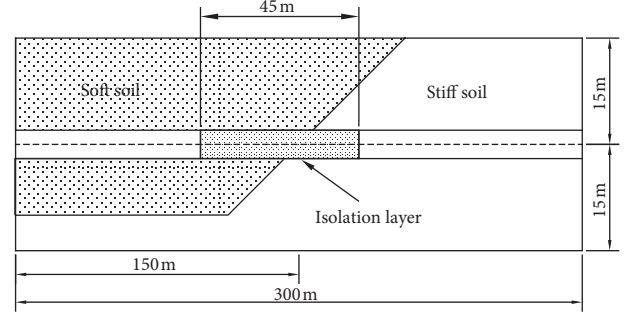


FIGURE 11: Ground and structure conditions in numerical simulations.

TABLE 1: Equivalent stiffness of the shield tunnel.

Segment ring width	$L_s$	m	1.0
Segment sectional area	$A_s$	$m^2$	3.81
Segment sectional inertia moment	$I_s$	$m^4$	11.23
Segment elastic modulus	$E_s$	kPa	$3.75 \times 10^7$
Sum of tension stiffness of ring joints	$K_j$	kN/m	$4.83 \times 10^6$
Equivalent compression stiffness	$(EA)_{eq}^C$	kN	$1.43 \times 10^8$
Equivalent tension stiffness	$(EA)_{eq}^T$	kN	$4.67 \times 10^6$
Equivalent bending stiffness	$(EI)_{eq}$	$kN \cdot m^2$	$3.59 \times 10^{15}$

its Poisson's ratio is close to 0.5. It meets requirements for grouting material. After being hardened, there is no harmful ingredient, nor does it pollute underground water. Table 2 reports the parameters for the SISMO silicone isolation material.

One-dimensional site response analysis based on the multireflection theory for layered soil (termed as the multireflection analysis) is conducted using the equivalent linear technique in this paper. The site responses as a free field are calculated, and the equivalent seismic rigidity and damping of the layered soil are obtained. The equivalent seismic rigidity of the soil deposits in Table 3 is used in every seismic analysis hereafter. The calculated accelerations are then applied to the axisymmetric finite element model.

**3.2.1. Longitudinal Direction.** Figures 14(a) and 14(b) show a comparison of the analysis results for the tunnel lining axial strains and stresses. Evidently, the axial peak strain and stress decrease after implementing the isolation layer. Table 4 indicates a decreased rate of axial strain and stress corresponding to different shear modulus. The lower the shear modulus of the isolation material, the better the isolation effect of the isolation layer.

**3.2.2. Transverse Direction.** Figure 15(a) shows a comparison of the analysis results for the tunnel lining axial strains. After the isolation layer is added, the axial peak tension strain decreases slightly, and the axial peak compression strain increases slightly.

Figure 15(b) shows a comparison of the analysis results for the tunnel lining axial stresses. After the isolation layer is added, the axial peak tension stress decreases slightly, and the axial peak compression stress almost remains the same.

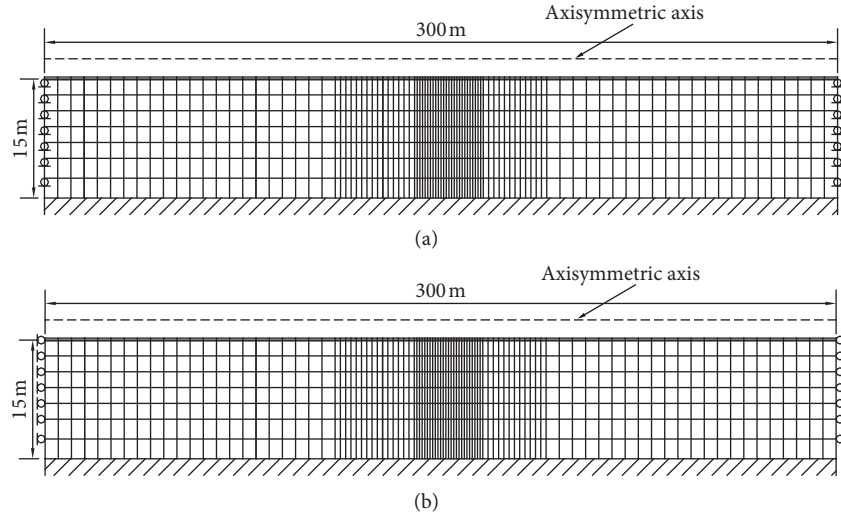


FIGURE 12: Discretization and boundary conditions of axisymmetric finite element mesh. (a) Longitudinal direction and (b) transverse direction.

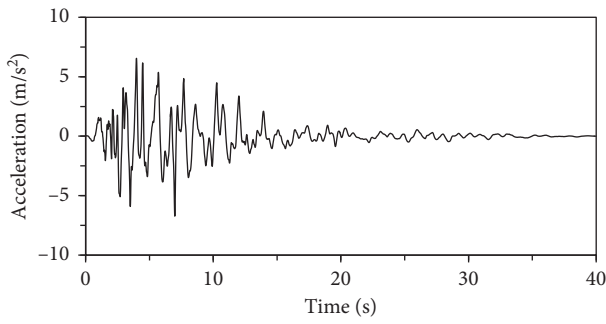


FIGURE 13: Time-acceleration curve.

TABLE 2: Mechanical parameters of SISMO material.

Material	Density (kg/m <sup>3</sup> )	Elastic modulus (MPa)	Poisson's ratio
SISMO-1	1200	0.1	0.48
SISMO-2	1200	0.3	0.48
SISMO-3	1200	0.5	0.48

TABLE 3: The equivalent seismic rigidity of soil deposits.

Material	Density (kg/m <sup>3</sup> )	Elastic modulus (MPa)	Poisson's ratio
Soft soil	1800	52.2	0.45
Stiff soil	2000	896	0.4

Therefore, when Poisson's ratio of isolation material is close to 0.5, the seismic isolation effect of isolation layer is not evident in the transverse direction.

**3.3. Research on Seismic Isolation Mechanism of Isolation Layers.** A spring is used to simulate the interaction between the seismically isolated tunnel and ground. Figures 16(a) and 16(b) show calculation models of the isolation layer spring

stiffness along the longitudinal and transverse directions of the tunnel, respectively. The calculation formula is as follows:

$$K_x = \frac{2\pi G}{\ln(R/r)},$$

$$K_y = \frac{8\pi G(3-4\nu)(1-\nu)}{(3-4\nu)^2 \ln(R/r) - [(R/r)^2 - 1]/[(R/r)^2 + 1]}, \quad (21)$$

$$t = R - r,$$

wherein  $K_x$  is the spring stiffness coefficient of the isolation layer along the longitudinal direction of a tunnel,  $K_y$  is the spring stiffness coefficient of the isolation layer along the transverse direction of a tunnel,  $R$  is the isolation layer outer diameter,  $r$  is the isolation layer inner diameter,  $G$  is the shear modulus of the isolation layer,  $\nu$  is Poisson's ratio of the isolation layer, and  $t$  is the thickness of the isolation layer.

Figure 17 shows how the shear modulus of isolation material affects the spring stiffness when Poisson's ratio is 0.48. As is known, the spring stiffness increase for both transverse and longitudinal tunnels with increased shear modulus. Figure 18 shows how Poisson's ratio affects the spring stiffness when the shear modulus is 0.3 MPa. When the shear modulus is constant, Poisson's ratio does not affect the spring stiffness of the isolation layer in the longitudinal direction, but the spring stiffness of the isolation layer in the transverse direction increases with increased Poisson's ratio. When Poisson's ratio is greater than 0.4, the increasing amplitude of spring stiffness increases sharply with increased Poisson's ratio.

For isolation material, the shear modulus should be relatively small, and Poisson's ratio is close to 0.5, avoiding ground settlement caused by the isolation layer. When the shear modulus is constant, Poisson's ratio does not affect the spring stiffness of the isolation layer along the

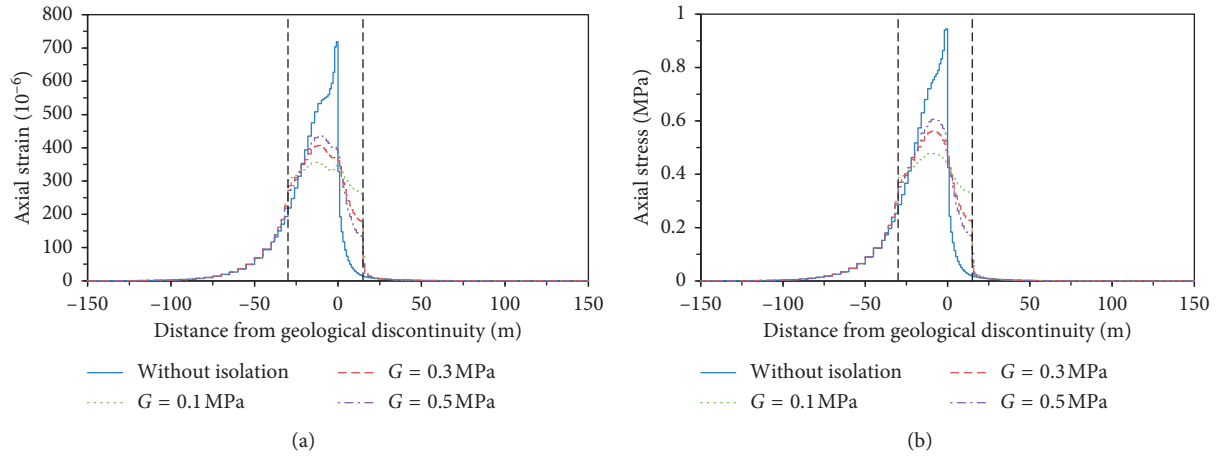


FIGURE 14: Analysis results along the longitudinal direction. (a) Axial strain and (b) axial stress.

TABLE 4: Decrease rate of axial peak strain and stress corresponding to different shear moduli.

Elastic modulus (MPa)	Decrease rate of peak strain (%)	Decrease rate of peak stress (%)
0.1	50.5	49.4
0.3	43.4	40.5
0.5	39.4	35.7

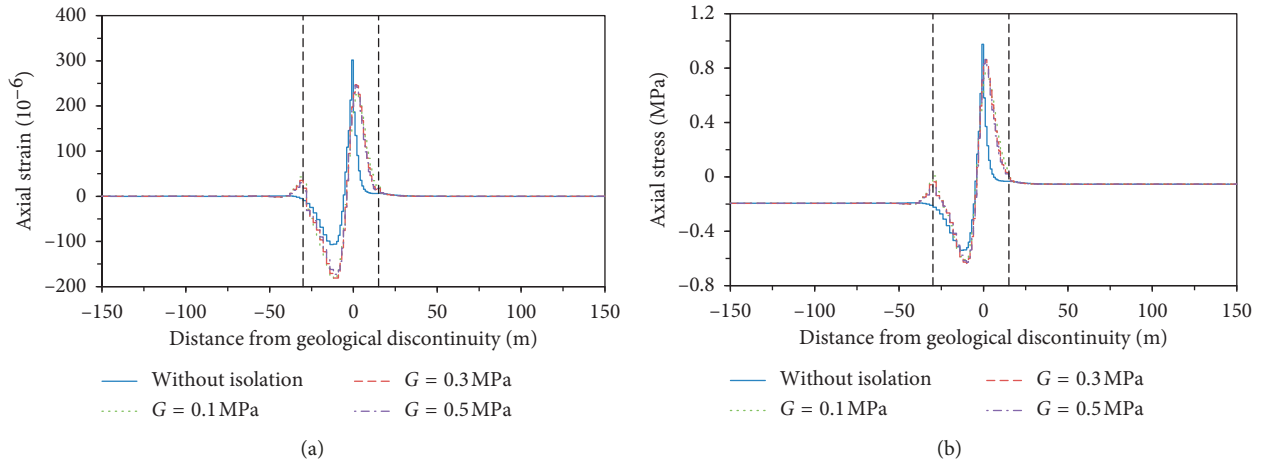


FIGURE 15: Analysis results along the transverse direction. (a) Axial strain and (b) axial stress.

longitudinal direction of a tunnel. When an isolation material with a small shear modulus is used, the tunnel is isolated from the deformation of its peripheral ground through the shear deformation of the isolation layer. A good isolation effect along the longitudinal direction of a tunnel is achieved. When Poisson’s ratio is close to 0.5, the spring stiffness is still great when an isolation material with small shear modulus is used, verifying that ground settlement can be avoided effectively when Poisson’s ratio is close to 0.5. However, the tunnel cannot be isolated from deformation of its peripheral ground through the compression deformation of the isolation layer. Therefore, a good isolation effect along the transverse direction of a tunnel cannot be achieved.

#### 4. Research on Seismic Isolation System of Shield Tunnel

Based on the above concept, the material used for the isolation layer in shield tunnels should have relatively low shear modulus, and its Poisson’s ratio should be approximately 0.5. However, the isolation layer cannot provide good isolation effect along the transverse direction of a tunnel. Considering that an earthquake would lead to concentration of stress at shaft joints and the positions at which ground conditions sharply change, flexible segments are correspondingly employed to increase the flexibility of the shield tunnel and improve its bending deformation capacity. However, there exist some difficulties in the layout of flexible

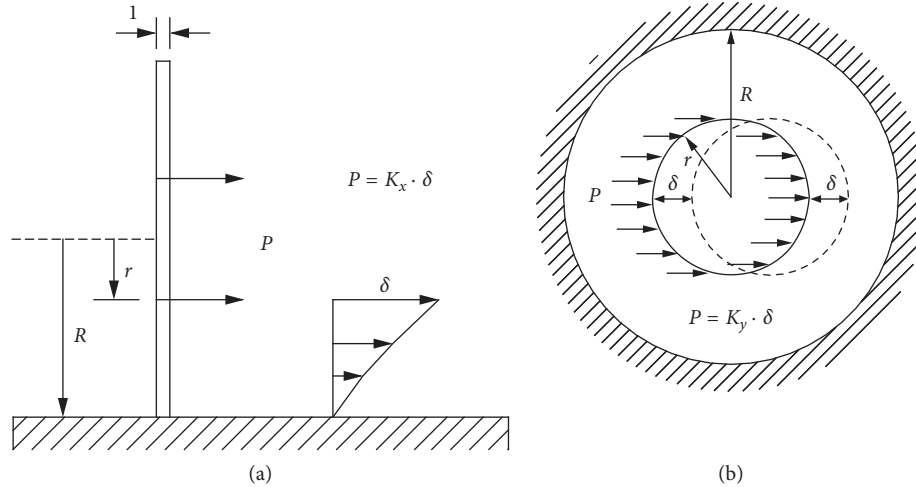


FIGURE 16: The model for calculating the isolation layer spring stiffness in (a) the longitudinal direction and (b) the transverse direction.

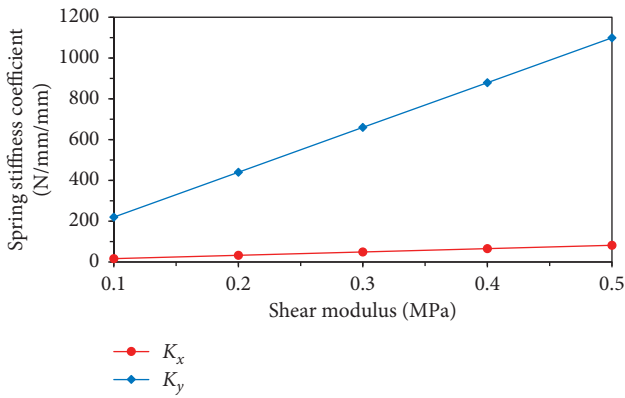


FIGURE 17: Effect of the shear modulus of the isolation material on the isolation layer spring stiffness.

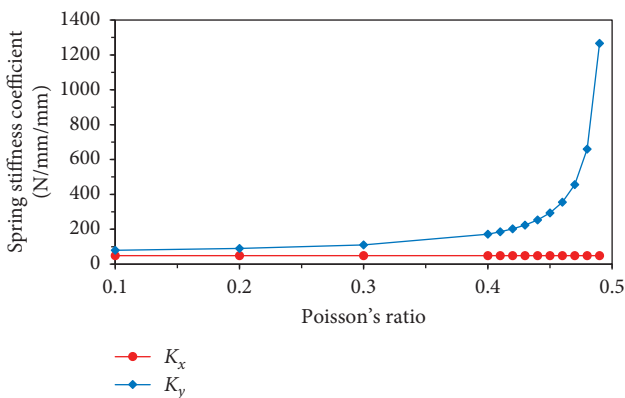


FIGURE 18: Effect of Poisson's ratio of the isolation material on the isolation layer spring stiffness.

segments owing to the uncertainty regarding the strain distribution in a shield tunnel when an earthquake occurs. Thus, a shield tunnel isolation system combining an isolation layer and flexible segments is proposed in this paper. As is shown in Figure 19, flexible segments are set at both ends of an isolation layer.

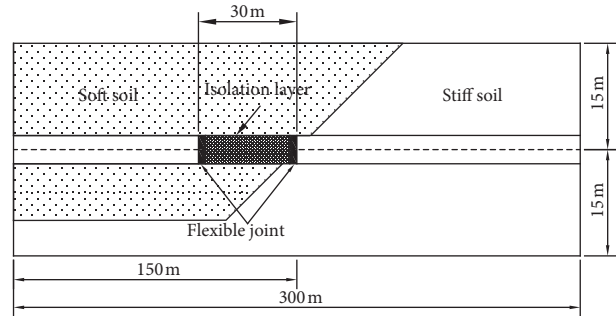


FIGURE 19: Shield isolation system for the shield tunnel.

The seismic responses of the shield tunnel along the longitudinal direction of the tunnel are shown in Figure 20(a). It is observed that when the seismic isolation system is built, the peak tension stress decreases to 47.9% of its original value and the stress distribution becomes smoother along the axial direction of the tunnel. On the contrary, the seismic responses of the shield tunnel along the transverse direction of the tunnel are represented in Figure 20(b). It is observed that when the axial peak tension stress decreases to 16.7% of its original value, the peak compression stress drops to 47.5% of its original value, and the stress distribution becomes smoother along the axial direction of the tunnel. Therefore, the proposed isolation system could have obvious effects on both longitudinal and transverse directions of a shield tunnel.

### 5. Conclusions

In this paper, a quasi-static method based on an axisymmetric finite element model for seismic response analysis of seismically isolated tunnels is used to research the seismic isolation effect and mechanism of seismic isolation layer of a shield tunnel along both longitudinal and transverse directions. The conclusions derived in this paper can be summarized as follows:

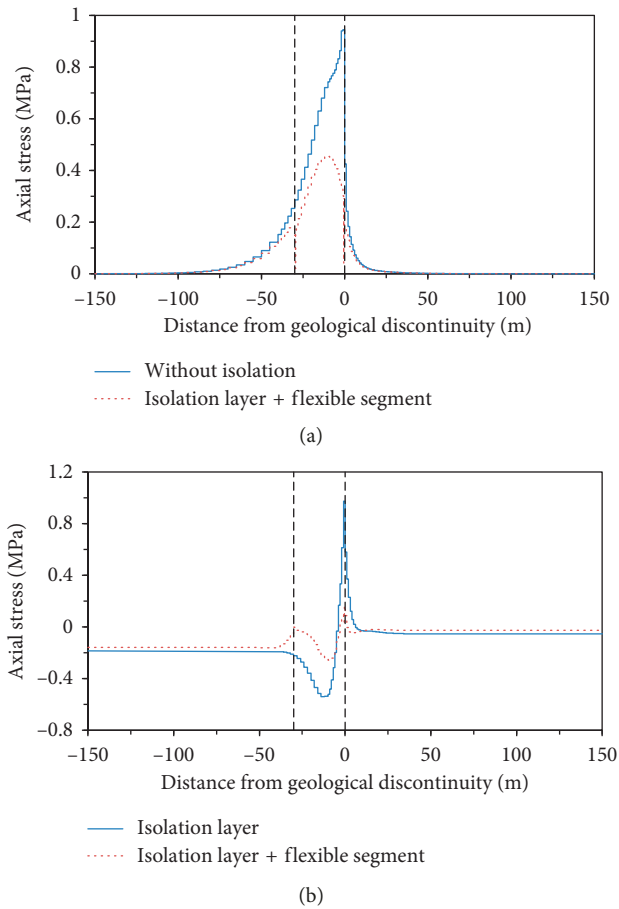


FIGURE 20: Seismic response of shield tunnel. (a) Longitudinal direction and (b) transverse direction.

- (1) Along the longitudinal direction of a tunnel, the seismic isolation effect of the elastic isolation layer is mainly affected by the shear modulus. The smaller the shear modulus of the isolation material, the better the isolation effect. This result occurs because the tunnel can be isolated from deformation of its peripheral ground through shear deformation of the isolation layer.
- (2) Along the transverse direction of a tunnel, the seismic isolation effect of the elastic isolation layer is mainly affected by the shear modulus and Poisson's ratio. When Poisson's ratio is approximately 0.5, the seismic isolation effect is not obvious. This result occurs because the tunnel cannot be isolated from the deformation of its peripheral ground through the compression deformation of the isolation layer.
- (3) A seismic isolation system for a shield tunnel in which flexible segments are arranged at both ends of an isolation layer is proposed. Based on the seismic response analysis, it is concluded that the system could have obvious effects on both the longitudinal and transverse directions of a tunnel.

## Data Availability

The data used to support the findings of this study are available from the corresponding author upon request.

## Conflicts of Interest

The authors declare that they have no conflicts of interest.

## Acknowledgments

The authors acknowledge the financial support received from the National Program on Key Basic Research Project of China (973 Program) (Grant no. 2015CB057906) and the National Key Research and Development Program of China (Grant no. 2018YFF01014204).

## References

- [1] Z. Y. Chen and H. Shen, "Dynamic centrifuge tests on isolation mechanism of tunnels subjected to seismic shaking," *Tunnelling and Underground Space Technology*, vol. 42, pp. 67–77, 2014.
- [2] W. S. Zhao, W. Z. Chen, X. J. Tan, and S. Huang, "Study on foamed concrete used as seismic isolation material for tunnels in rock," *Materials Research Innovations*, vol. 17, no. 7, pp. 465–472, 2014.
- [3] T. Suzuki and T. Tanaka, "Research and development on the seismic isolation system applied to urban tunnels (part-1: development of seismic isolation materials and construction methods)," in *Proceedings of the 7th U.S.-Japan Workshop on Earthquake Disaster Prevention for Lifeline Systems*, pp. 447–459, Seattle, WA, USA, November 1997.
- [4] T. Tanaka and T. Suzuki, "Research and development on the seismic isolation system applied to urban tunnels (part-2: effects of seismic isolation and seismic design)," in *Proceedings of the 7th U.S.-Japan Workshop on Earthquake Disaster Prevention for Lifeline Systems*, pp. 461–475, Seattle, WA, USA, November 1997.
- [5] W. Zhao, W. Chen, and D. Yang, "Interaction between strengthening and isolation layers for tunnels in rock subjected to SH waves," *Tunnelling and Underground Space Technology*, vol. 79, pp. 121–133, 2018.
- [6] M. N. Wang and G. Y. Cui, "Study of the mechanism of shock absorption layer in the supporting system of tunnels in highly seismic areas," *China Civil Engineering Journal*, vol. 44, no. 8, pp. 126–131, 2011.
- [7] K. Kawashima, *Seismic Design of Underground Structures*, Kajima Press, Tokyo, Japan, 1994.
- [8] T. Suzuki, "Comparison between finite element analysis and seismic displacement method on a transmission coefficient of seismic axial strain of shield-driven tunnels," *Journal of Japan Society of Civil Engineers, Ser. A1 (Structural Engineering & Earthquake Engineering (SE/EE))*, vol. 65, no. 1, pp. 236–243, 2009.
- [9] S. Huang, W. Z. Chen, J. P. Yang et al., "Research on earthquake-induced dynamic responses and aseismic measures for underground engineering," *Chinese Journal of Rock Mechanics and Engineering*, vol. 28, no. 3, pp. 483–490, 2009.
- [10] W. S. Zhao, W. Z. Chen, S. S. Ma et al., "Isolation effect of foamed concrete layer on seismic responses of tunnel," *Rock and Soil Mechanics*, vol. 39, no. 2, pp. 1027–1036, 2018.

- [11] Y. M. A. Hashash, J. J. Hook, B. Schmidt, and J. I-Chiang Yao, "Seismic design and analysis of underground structures," *Tunnelling and Underground Space Technology*, vol. 16, no. 4, pp. 247–293, 2001.
- [12] I. Katayama, M. Adachi, Y. Shimada et al., "Proposal of practical quasi-dynamic analysis method for underground structures named response acceleration method," *Proceedings of the 40th Annual Meeting of JSCE*, vol. 369, pp. 737–738, 1985.
- [13] I. Katayama, *Studies on Fundamental Problems in Seismic Design Analyses of Critical Structures and Facilities*, Ph.D. thesis, Kyoto University, Kyoto, Japan, 1990.
- [14] A. Tateishi, "A study on seismic analysis methods in the cross section of underground structures using static finite element method," *Structural Engineering/Earthquake Engineering*, vol. 22, no. 1, pp. 41s–54s, 2005.
- [15] T. Suzuki and M. Maruyama, "The axisymmetric finite element model developed as a measure to evaluate earthquake response of seismically isolated tunnels," in *Proceedings of the 10th Japan Earthquake Engineering Symposium*, pp. 2003–2008, Tokyo, Japan, 1998.
- [16] T. Suzuki, "The axisymmetric finite element model developed as a measure to evaluate earthquake response of seismically isolated tunnels," in *Proceedings of the 12th World Conference on Earthquake Engineering*, Auckland, New Zealand, September 2000.
- [17] Japan Road Association, *Specifications of Highway Bridges (Part-V: Seismic Design)*, Maruzen Press, Tokyo, Japan, 2012.
- [18] T. Suzuki and C. Tamura, "Proposal of a seismic isolation structure for urban tunnels and the method to evaluate its isolation effects," *Doboku Gakkai Ronbunshu*, vol. 525/I-33, no. 525, pp. 275–285, 1995.

